

NONLINEAR STRUCTURAL ANALYSIS FOR FIBER-REINFORCED SUPERALLOY TURBINE BLADES

D. A. Hopkins and C. C. Chamis
Structures and Mechanical Technologies Division
NASA Lewis Research Center
Cleveland, Ohio 44135

Abstract

A computational capability for predicting the nonlinear thermomechanical structural response of fiber-reinforced superalloy (FRS) turbine blades is described. This capability is embedded in a special-purpose computer code recently developed at the NASA Lewis Research Center. Special features of this computational capability include accounting for; fiber/matrix reaction, nonlinear and anisotropic material behavior, complex stress distribution due to local and global heterogeneity, and residual stresses due to initial fabrication and/or inelastic behavior during subsequent missions.

Numerical results are presented from analyses of a hypothetical FRS turbine blade subjected to a fabrication process and subsequent mission cycle. The results demonstrate the capabilities of this computational tool to; predict local stress/strain response and capture trends of local nonlinear and anisotropic material behavior, relate the effects of this local behavior to the global response of a multilayered fiber-composite turbine blade, and trace material history from fabrication through successive missions.

Introduction

Fiber-reinforced superalloys (FRS) are becoming more attractive for hot-section applications in aircraft gas turbine and liquid-propellant rocket engines. Recently, specific investigations¹⁻³ have focused on the benefit of using FRS for components (rotor blades) of aircraft engine high-pressure

turbines and Space Shuttle Main Engine high-pressure fuel turbopumps. In short, these investigations demonstrated, qualitatively at least, the potential of FRS to provide a substantial improvement in component durability and maximum temperature capability beyond that presently achieved with monolithic materials.

Despite the apparent advantages of FRS, the prospects for having a production engine with FRS turbine components in the near future are remote. This is largely due to the fact that no adequate (accurate and economical) means currently exist for making a quantitative assessment of the mechanical performance and structural integrity of composite materials in such complex structural applications as turbine blades. The availability of adequate structural analysis/design tools is imperative if the use of FRS, or any advanced composite material, for engine hot-section components, or any complex structural application, is to become a reality.

In response to the deficiency mentioned above, research is being conducted at the NASA Lewis Research Center to develop computational nonlinear structural mechanics methodologies for high-temperature composite engine structures. One recent result of these efforts has been the development of a computational capability specifically tailored for the nonlinear structural/stress analysis of FRS turbine blades.⁴ The intent here is to provide a brief and general overview of this analytical tool together with some typical results obtained from a recent exercise using this capability.

Computational Capability

Clearly, the utility of any structural analysis tool depends on the accuracy with which it describes or predicts the actual physical event being modeled. In this light, the primary goal in developing the computational capability mentioned above was to account for the physics governing this application

in the analytical formulation of the problem. In doing so, it was assumed that the behavior of a FRS turbine blade could be predominantly attributed to certain physical characteristics and/or phenomena associated with this application, including;

- local (intralaminar) heterogeneity of a fiber-reinforced composite ply
- global (interlaminar) heterogeneity of a multilayered angleplied composite structure
- fiber/matrix metallurgical reaction due to extended exposure in elevated temperature environments
- nonlinear (stress-temperature-time dependent) and anisotropic constituent material behavior due to complex and cyclic thermomechanical loading conditions
- complex and nonuniform microstress distribution in the composite constituents due to intralaminar heterogeneity and anisotropic nonlinearities
- residual stresses due to initial composite fabrication process and/or inelastic behavior during subsequent mission cycles

Accountability of these factors, then, was judged to be most critical to the development of an appropriate and adequate structural analysis tool.

To develop the computational capability alluded to above, the existing COBSTRAN computer code was used as a foundation. COBSTRAN (COmposite Blade STRuctural ANalysis) is a special-purpose code developed several years ago at the NASA Lewis Research Center to perform linear-elastic structural analysis of composite blade-like structures. This recently developed nonlinear version of COBSTRAN is an integrated structural analysis tool incorporating; a

fiber degradation model, a nonlinear material model/cumulative damage model, composite micromechanics theory, laminate theory, and global finite element structural analysis.

The analytical procedure of nonlinear COBSTRAN is based on an incremental/iterative solution strategy. This strategy entails the successive solution of a linear formulation for distinct increments of the total load/time domain of the problem. During the process, results from the solution of each load/time increment are used to update the problem formulation for solution of the next increment. In this manner, the solution strategy embedded in nonlinear COBSTRAN resembles the forward-Euler type scheme.⁵

As implemented in nonlinear COBSTRAN, the solution strategy described above involves two levels of iteration. The primary iteration occurs for the load/time stepping process. For each distinct increment then, the secondary iteration occurs to achieve convergence at an equilibrium solution. Presently, a criterion based on the error in nodal displacement components for successive iterations is used to establish equilibrium-solution convergence.

The functional essence of the computational capability embodied by nonlinear COBSTRAN is depicted graphically in Figure 1. The schematic summarizes the major elements comprising this integrated structural analysis tool while the circular arrangement portrays the iterative nature of the solution strategy. Moreover, a distinct computational "hierarchy" is evident from the schematic. In other words, there is a clear progression from a description of material properties at the "micro" level to a prediction of structural response at the "macro" level, and back. In short, the analytical process illustrated in Figure 1 can be described as an "upward integration" of the structural analysis model and a "downward decomposition" of the structural response variables.

As implied in Figure 1, the problem of material nonlinearity is treated at the lowermost level in the computational hierarchy i.e., in the constituent materials comprising each ply. To describe the nonlinear material behavior, a simple thermoviscoplastic constitutive model was formulated on the premise that the nonlinearity could be expressed in terms of a stress-temperature-time dependency of the constituent material properties. As such, the model relates the incremental stress in the constituent to the incremental strain in a manner similar to the Hooke's Law relationships. However, in this case the material properties are taken to be dependent functions of stress, stress-rate, temperature, and time. The material model also incorporates a simple cumulative damage/life fraction model based on the concept of residual strength.

The fiber/matrix reaction phenomenon is accounted for in conjunction with the treatment of material nonlinearity. An empirical expression is used to quantify the reduction in cross-sectional area of the intact fibers. The resulting growth of an interphase of material between the intact fiber and matrix is accommodated by providing for the separate characterization of this material as an additional constituent of the ply.

Composite micromechanics theory and laminate theory comprise the two intermediate levels in the computational hierarchy depicted in Figure 1. In effect, the two theories constitute an idealization of the inherently heterogeneous composite structure as an equivalent "pseudo-homogeneous" one. In the upward integration process these theories provide the means to predict equivalent properties of a pseudo-homogeneous finite element based on the properties of the constituent materials and the geometrical characteristics of the composite (ply and laminate). In the downward decomposition process the theories provide the means to relate the global response of the composite structure back to the local response of the individual constituents of each ply.

Global structural analysis by the finite element method (FEM) represents the uppermost level of the computational hierarchy illustrated in Figure 1. A superficial summary of the governing equations of linear structural analysis, from a FEM perspective, is given in Figure 2. Part of the analytical process of nonlinear COBSTRAN involves solution of these equations for each successive increment of the total load/time domain of the problem, as depicted in the accompanying schematic. At present, the nonlinear COBSTRAN code interfaces with the MSC/NASTRAN⁶ code for global FEM structural analysis requirements.

Turbine Blade Analyses

In an effort to demonstrate the utility and capabilities of the integrated structural analysis tool described above, some typical results are given below from a recent exercise involving analyses of a hypothetical FRS turbine blade airfoil. The analyses were conducted to investigate the effects on the airfoil of a fabrication process and the subsequent response of the airfoil to a mission cycle.

An illustration of the airfoil geometry used in the analyses is given in Figure 3. Overall, the approximate dimensions of the airfoil are; 2.15 in. along the span, 1.20 in. across the chord, and 0.040 in. through-the-thickness of the wall. The airfoil has a slight axial twist and a tapered cross-section from root to tip. The discretized finite element model of the airfoil shown in Figure 3 contains 220 quadrilateral isoparametric membrane-bending elements and 240 nodal points (1200 degrees-of-freedom less those constrained by imposed boundary conditions).

A summary of the specific FRS composite system used for the analyses is also given in Figure 3. The system entails a 4-ply laminate with a configuration of $[\pm 45^\circ]_S$. The individual plies are 0.010 in. thick and consist of Fe-25Cr-4Al-1Y matrix reinforced with 0.008 in. diameter continuous W-1.5ThO₂ fibers yielding a fiber volume fraction of 0.50.

The objective of the first analysis of the FRS airfoil was to investigate the residual stress state induced by thermal loading experienced during a fabrication process. The process simulated for the analysis was adapted from an actual hot isostatic pressing (HIP) process used in the fabrication of laboratory test specimens. The complete HIP process consists of; a 20-minute heat-up transient (room temperature to 1950° F), a 30-minute constant temperature/pressure transient (1950° F/15,000 psi), and a 16-hour cool-down transient (1950° F to room temperature).

The analysis of the fabrication process simulated only the cool-down portion of the HIP process inasmuch as the transition from the constant temperature/pressure transient to the cool-down transient was judged to be a reasonable point in the process to assume the onset of composite behavior. Moreover, it was assumed that the individual plies were being consolidated simultaneously with the fabrication of the airfoil in order to neglect the existence of any initial residual microstress in the ply constituents prior to component fabrication.

The cool-down transient, illustrated in Figure 4, was simulated using 30 load/time increments. The temperature was assumed to be uniform over the entire airfoil (spanwise, chordwise, and through-the-thickness). Boundary conditions for the analysis were specified so as to provide immobility of the airfoil model with minimal constraint. A maximum error tolerance of one percent was prescribed for the equilibrium-solution convergence criterion. The analysis required a total of 61 iterations and consumed approximately 20 minutes of CPU time on a Cray 1S computer system.

Results from the analysis of the fabrication cool-down process indicated a practically uniform state of ply residual stress throughout the airfoil, as anticipated in view of the uniform temperature distribution and "quasi-isotropic" ply configuration.

Magnitudes of longitudinal normal ply stress, σ_{L11} (see ply coordinate system, Figure 5), varied from -11.5 ksi to -13.4 ksi with the majority of values falling in the range -12.5 ± 0.3 ksi. Magnitudes of transverse normal ply stress, σ_{L22} , were similar to σ_{L11} but of opposite sense, i.e. tensile rather than compressive. Also evident were ply in-plane shear stresses, σ_{L12} , ranging in magnitude from 0.0 to ± 0.4 ksi. These small shear stresses and the deviation in normal stresses are attributed primarily to small-scale local bending and/or twisting of the airfoil due to the asymmetric airfoil geometry.

The build-up of residual stress in a ply and the resulting microstress state in the ply constituents throughout the duration of the cool-down process is illustrated in Figure 5. These results are of the longitudinal normal stress/microstress (σ_{11}) in the outermost ($+45^\circ$) ply and its constituents at a location on the airfoil corresponding to the root leading edge point (see arrow, Figure 4). What is noteworthy about the results illustrated in Figure 5 is that, despite a relatively low magnitude of ply stress, the constituent constituent microstress magnitudes are quite large. This reflects the substantial contribution of thermally induced microstress due to the mismatch in thermal expansion characteristics of the two materials.

Similar to Figure 5, results are presented in Figure 6 of transverse normal stress/microstress (σ_{22}) for the same ply at the same airfoil location. Different from σ_{11} however, the interaction of constituents in the transverse direction causes the distribution of σ_{22} (and σ_{12}) in the matrix and interphase to be nonuniform through-the-thickness of the ply. This intraply nonuniformity is characterized by three distinct regions (A-B-C) as shown in the schematic. A review of the results for matrix microstress, for example, indicates the significance of this intraply nonuniformity. A transition occurs from a tensile microstress in regions A and B to a compressive microstress in region C.

One ramification of the intraply nonuniformity of σ_{22} (and σ_{12}) for the matrix and interphase concerns the potential for the microstress in a select region to exceed the yield point of the material. This localized inelastic behavior would result in an induced anisotropy of the material that serves to exacerbate the already complex physical characteristics of this problem. With this in mind, it is easier to envision how local flaws might initiate, propagate, and eventually cause complete failure in a turbine blade, for example. The point to be taken from this is the importance of being able to account for behavior on the "micro" scale, and therein lies the utility of the integrated computational capability embodied by nonlinear COBSTRAN.

The second analysis of the FRS turbine blade airfoil was conducted to investigate the response to the thermal, pressure, and centrifugal loads experienced during a mission cycle. Complete details of the loading conditions are excluded here for the sake of brevity and because they are unimportant within the scope of this discussion. It will suffice to say that the temperature and pressure distributions over the airfoil surfaces (pressure and suction) had a bicubic variation (spanwise and chordwise) throughout the mission cycle.

The mission cycle was simulated with 43 load/time increments. The imposed boundary conditions most closely represented those of a cantilevered structure. The same maximum error tolerance of one percent was prescribed for the convergence criterion. The analysis required a total of 112 iterations and consumed approximately 50 minutes of CPU time.

Results from the mission cycle analysis indicated an overall change in the ply residual stress state from prior (initial fabrication residual stresses) to after the mission. In general, the magnitudes of σ_{L11} were decreased for all plies while the magnitudes of σ_{L22} were increased for all plies. In all cases σ_{L11} remained compressive and σ_{L22} remained tensile.

The extent of this change in ply residual stress magnitude varied depending on the location on the airfoil. For example, the change was most noticeable at the root section and least noticeable at the tip, as might be expected since the effects of the pressure and centrifugal loads vanish at the tip. Likewise, the change was more significant at mid-chord, and especially on the suction surface, than at the leading or trailing edges. As an illustration, the maximum ply residual stress at the end of the mission cycle was approximately +19.0 ksi and occurred in the σ_{22} component for the outermost ply on the suction surface at the root mid-chord location.

Results similar to those shown earlier for the analysis of the fabrication cool-down process are presented now for the mission cycle analysis, using the same ply at the same airfoil location (outermost ply, root leading edge). Figures 7 through 9 illustrate the temperature, pressure, and centrifugal load variations, respectively, throughout the mission for this location. Figure 10 illustrates the variation of longitudinal tensile strength (S_{11T}) in the constituents and for the ply. These results reflect a dependence of strength on primarily temperature. Figure 11 illustrates the variation of stress/microstress magnitude throughout the mission.

The first point to note from the results shown in Figures 7 through 11 is the large variation in the constituent microstress state despite a relatively constant ply stress. Again, this reflects the contribution of thermally induced microstress due to the mismatch in thermal expansion characteristics of the two materials. Secondly, and perhaps most intriguing, is that the microstress state is minimum at maximum load conditions and when available strength in the constituents is minimum. This suggests a potential design flexibility which is unique to composite material systems.

A final result from the analysis of the mission cycle is illustrated in Figure 12 showing the

variation throughout the mission of natural vibration frequencies for the airfoil. The results reflect the change in frequency corresponding to the change in stiffness of the airfoil, due initially to the variation in temperature and then to the inelastic deformation in the airfoil.

Conclusions

The numerical results presented above serve as examples of the type of information provided by the nonlinear COBSTRAN code. The results demonstrate the unique capabilities of this computational tool to relate local nonlinear constituent material behavior to the global response of an FRS composite turbine blade. Moreover, the results manifest the utility of the "upward integration/downward decomposition" approach, in general, for nonlinear structural analysis of any composite structure.

References

1. P. Melnyk and J. N. Fleck, "Tungsten Wire Reinforced Superalloys for 1093 C (2000° F) Turbine Blade Applications", NASA CR-159720, 1979.
2. D. W. Petrasek and R. A. Signorelli, "Tungsten Fiber Reinforced Superalloys - A Status Review", NASA TM-82590, 1981.
3. J. R. Lewis, "Design Overview of Fiber Reinforced Superalloy Composites for the Space Shuttle Main Engine", NASA CR-168185, 1983.
4. D. A. Hopkins, "Nonlinear Analysis for High-Temperature Multilayered Fiber Composite Structures", NASA TM-83754, 1984.
5. O. C. Zienkiewicz, The Finite Element Method, 3rd ed., McGraw-Hill Book Company (UK) Limited, London, 1977.

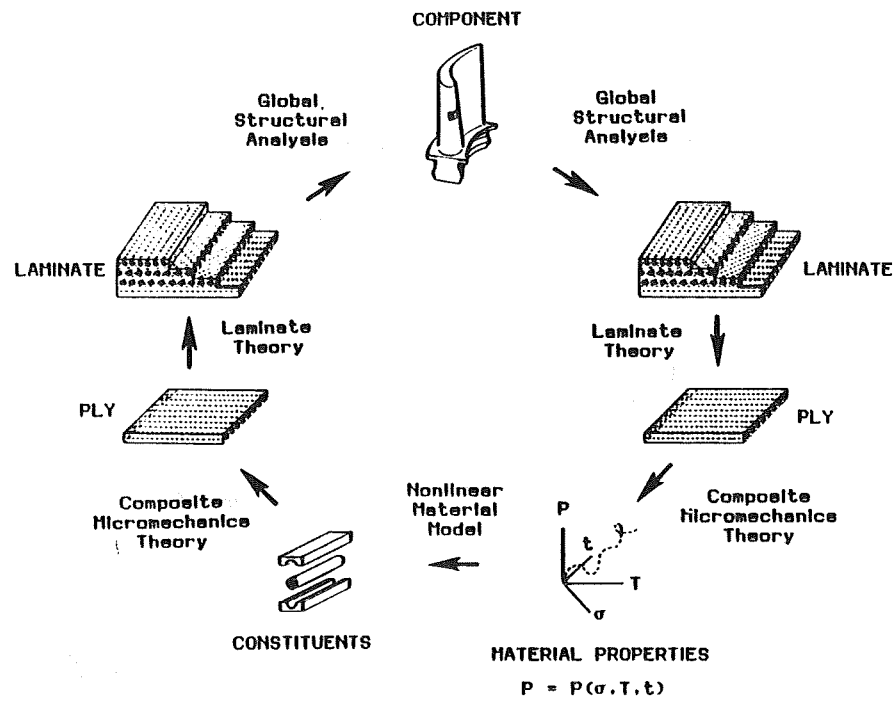


Figure 1 - Integrated Approach to Nonlinear Structural Analysis of FRS Turbine Blades

$$[M]\{\ddot{u}\} + [C]\{\dot{u}\} + [K]\{u\} = \{F(t)\}$$

$$\langle [K] - \lambda[M] \rangle \{u\} = \{0\} \rightarrow \{\omega_n\}$$

$$\{u\} \leq \{u_a\}$$

$$\{\sigma\} = [E][B]\{u\} \leq \{S_a\}$$

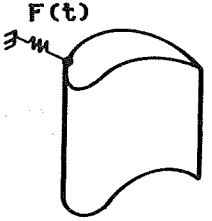
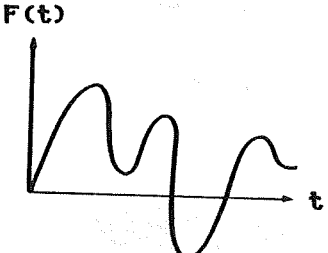
$$\{\omega\} \leq \{\omega_a\}$$



Figure 2 - Summary of Governing Equations for Global Linear Structural Analysis

$WThO_2/FeCrAlY$

$\nu_f = 0.50$

$t_1 = 0.010''$

$\theta = [\pm 45]_g$

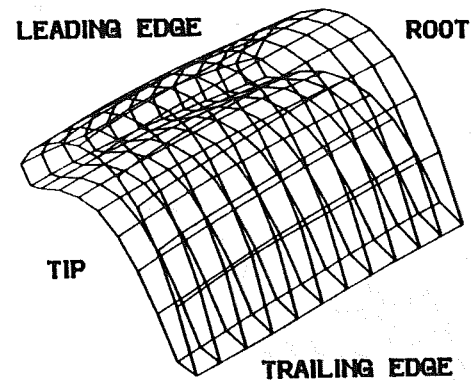


Figure 3 - FRS Turbine Blade Model and Material System

NODE NO. 11
PLY NO. 1

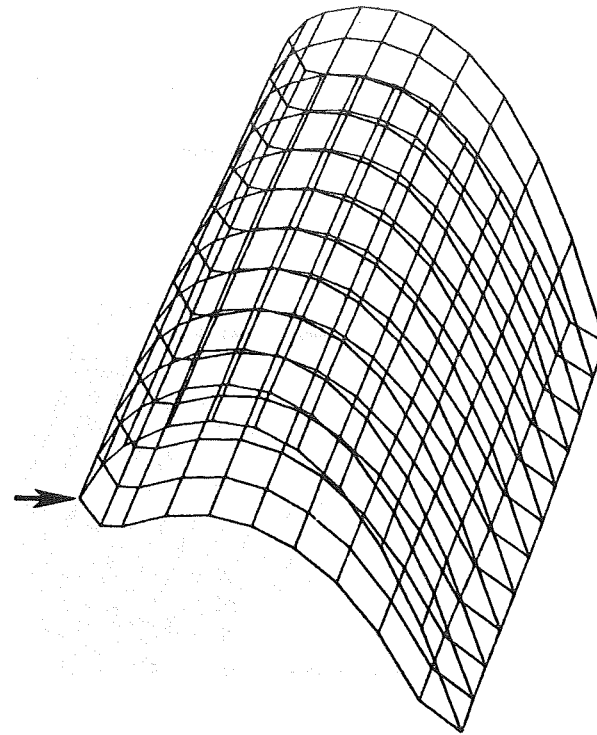
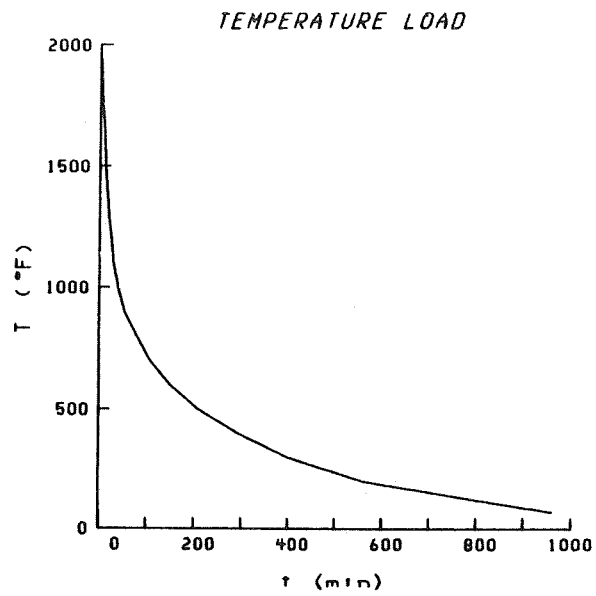
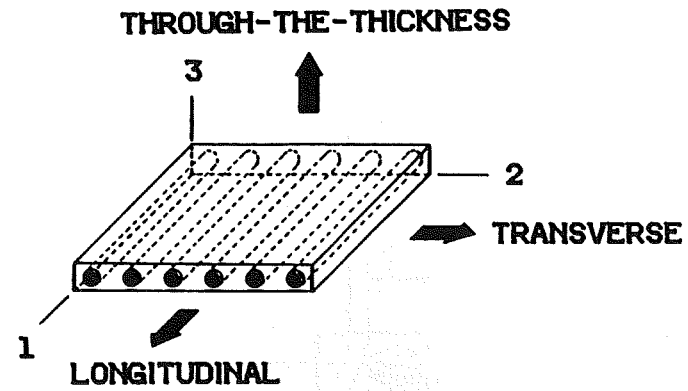
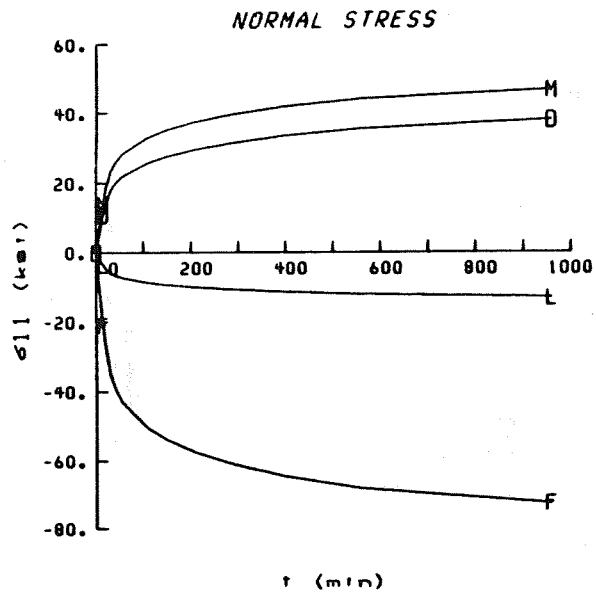


Figure 4 - Fabrication Cool-Down Process and Airfoil
Root Leading Edge Location

NODE NO. 11
PLY NO. 1

F FIBER
M MATRIX
D INTERPHASE
L PLY



333

Figure 5 - Fabrication Residual Stress/Microstress (σ_{11})
Build-up and Ply Coordinate System

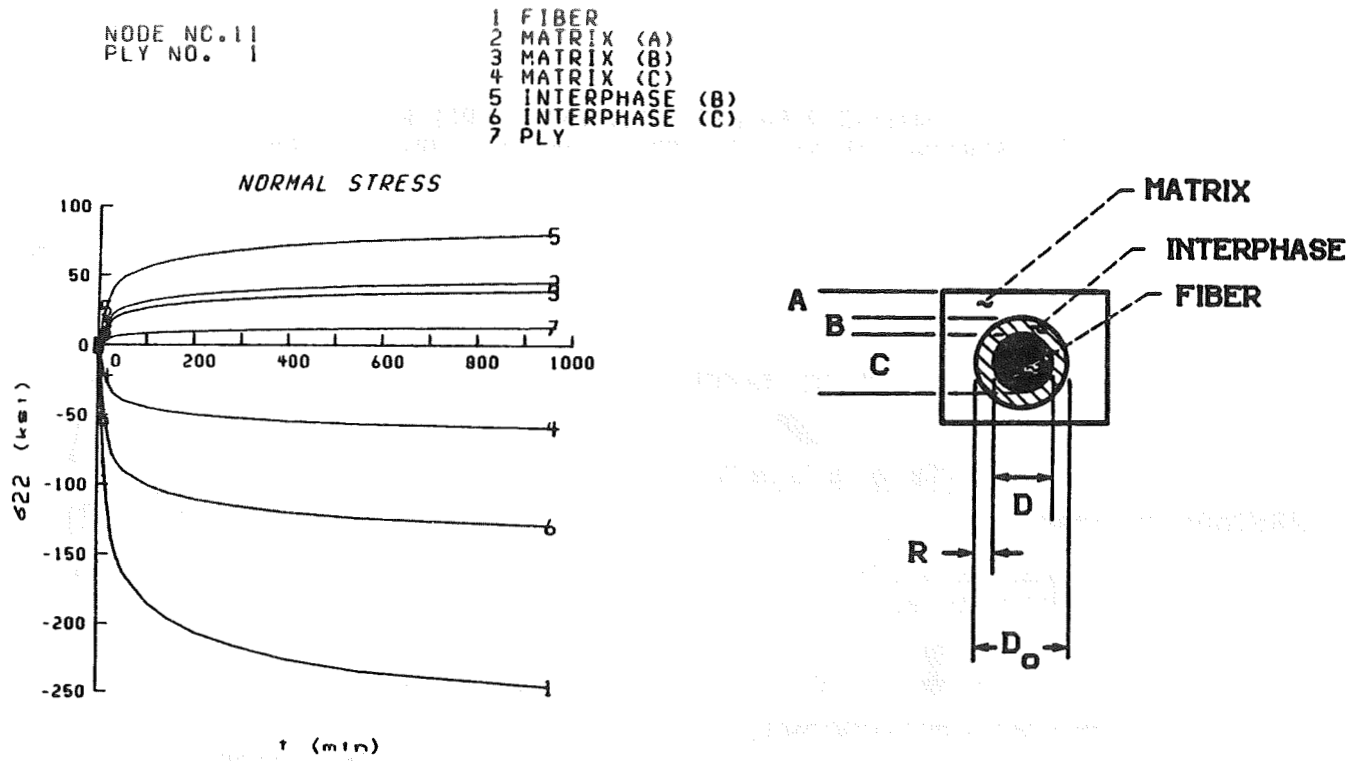


Figure 6 - Fabrication Residual Stress/Microstress (σ_{22}) Build-up and Regions (A-B-C) of Nonuniformity

NODE NO.11
PLY NO. 1

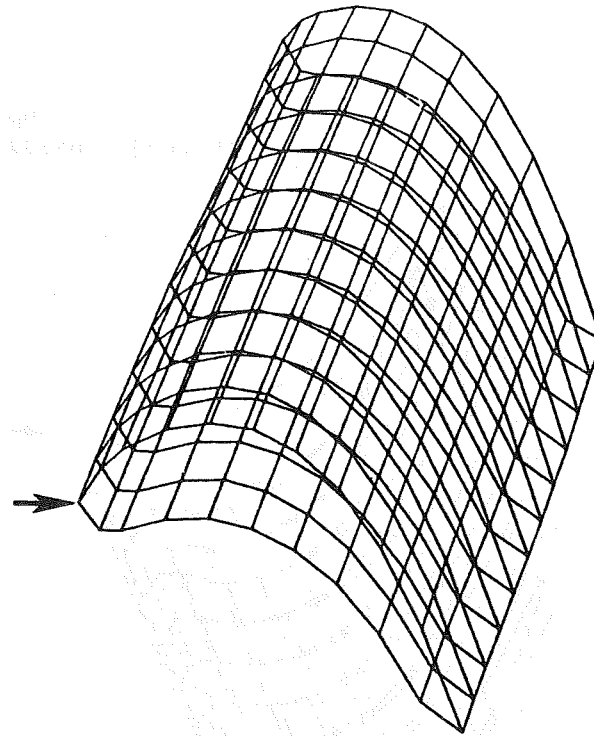
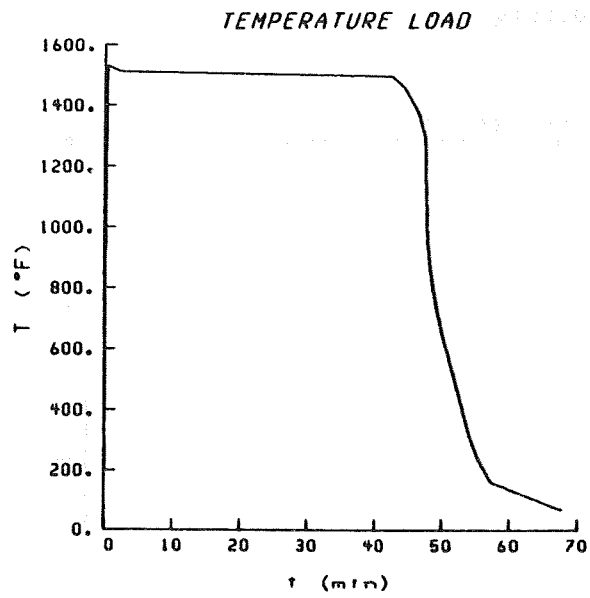


Figure 7 - Mission Cycle Temperature Load at Root Leading Edge

NODE NO. 11
PLY NO. 1

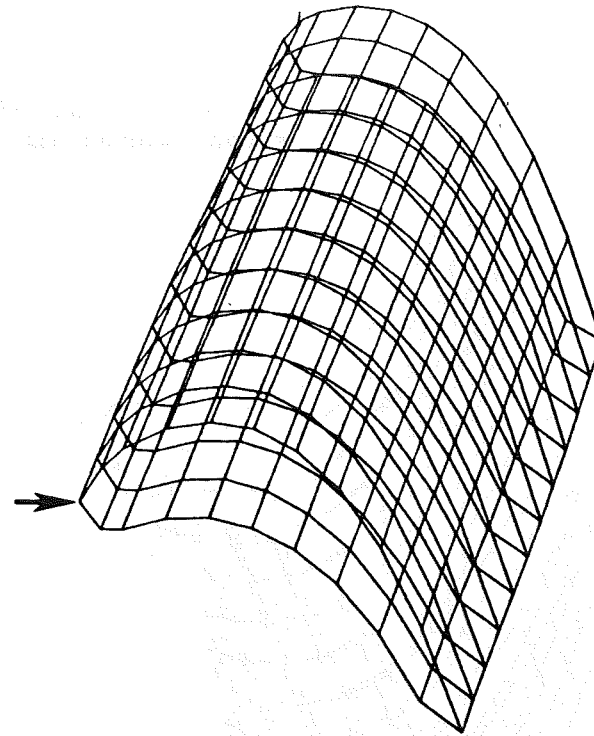
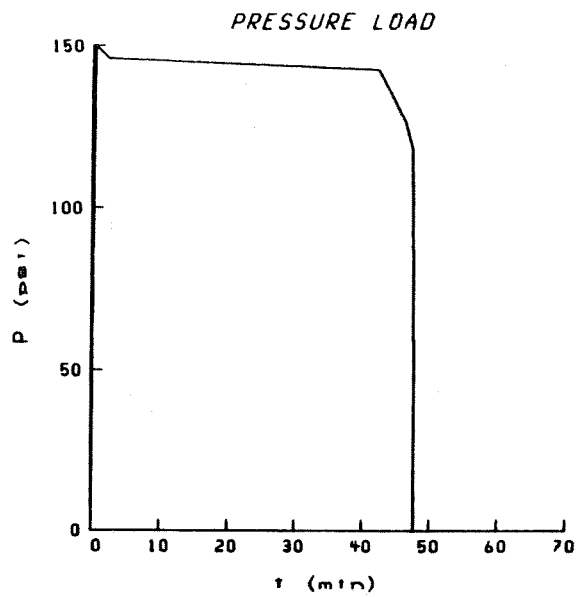
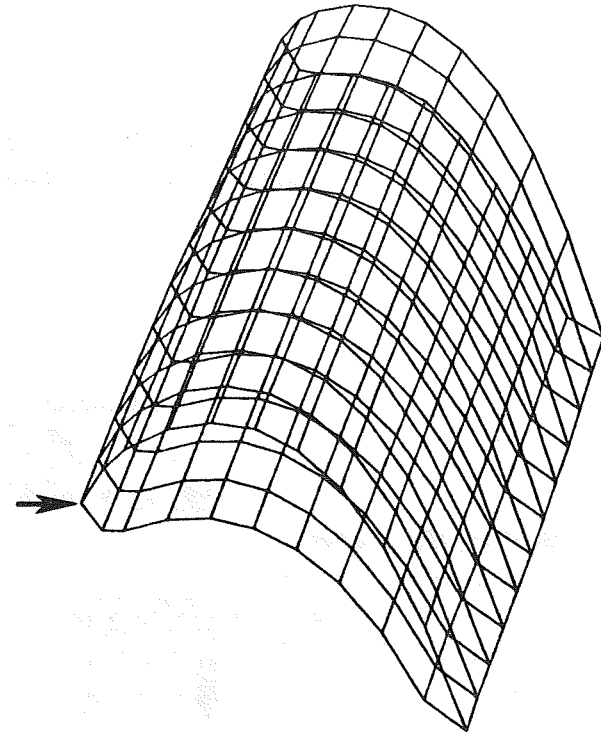
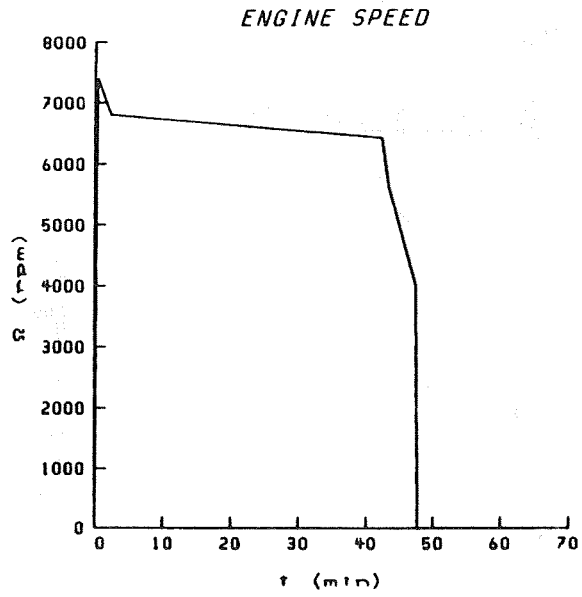


Figure 8 - Mission Cycle Pressure Load at Root Leading Edge

NODE NO. 11
PLY NO. 1



337

Figure 9 - Mission Cycle Engine Speed

NODE NO. 11
PLY NO. 1

F FIBER
M MATRIX
D INTERPHASE
L PLY

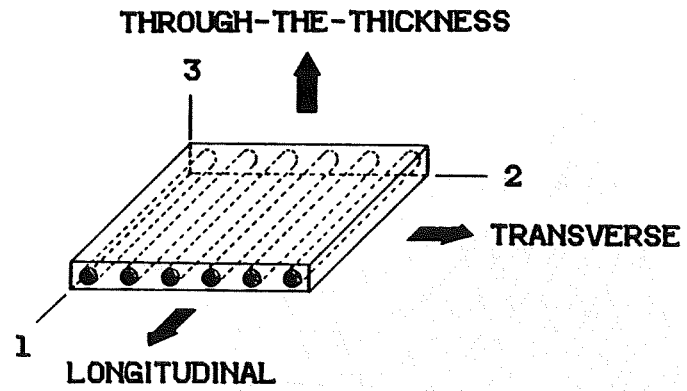
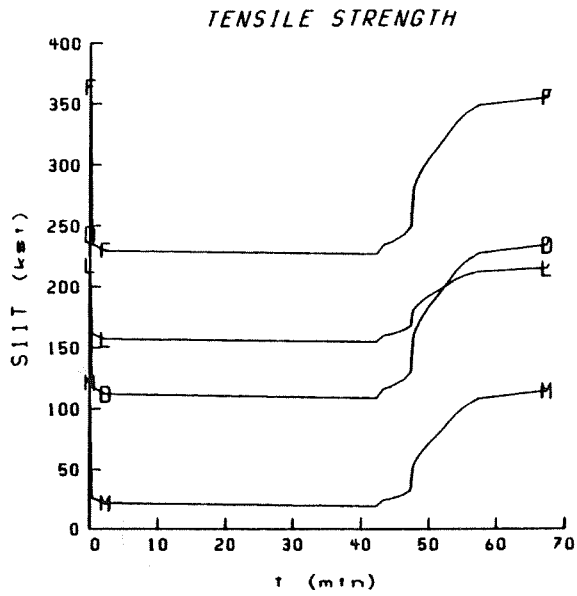


Figure 10 - Variation of Longitudinal Tensile Strength (S_{11T})

NODE NO.11
PLY NO. 1

F FIBER
M MATRIX
D INTERPHASE
L PLY

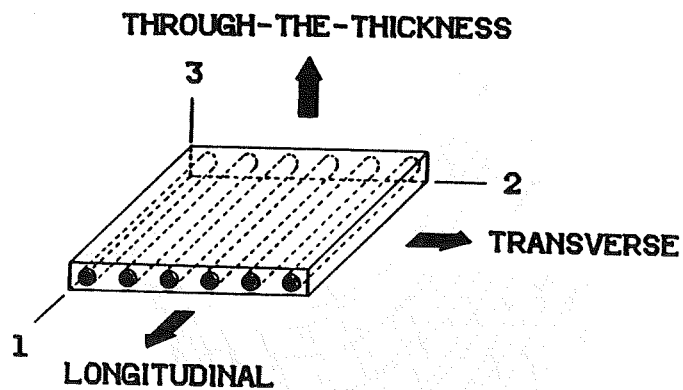
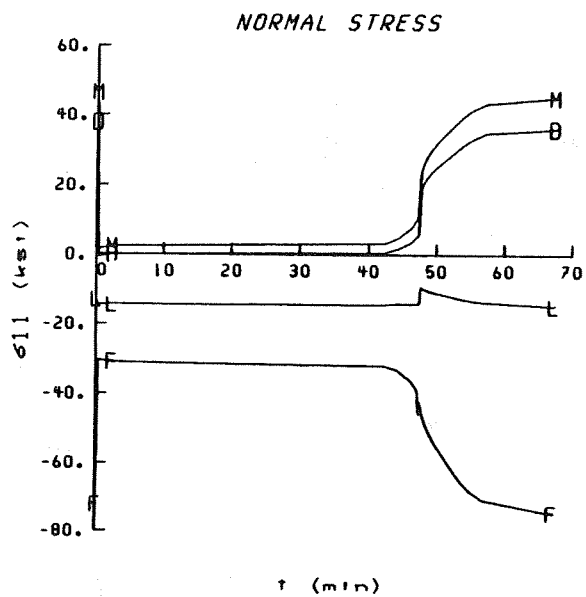


Figure 11 - Variation of Longitudinal Normal Stress/Microstress (σ_{11})

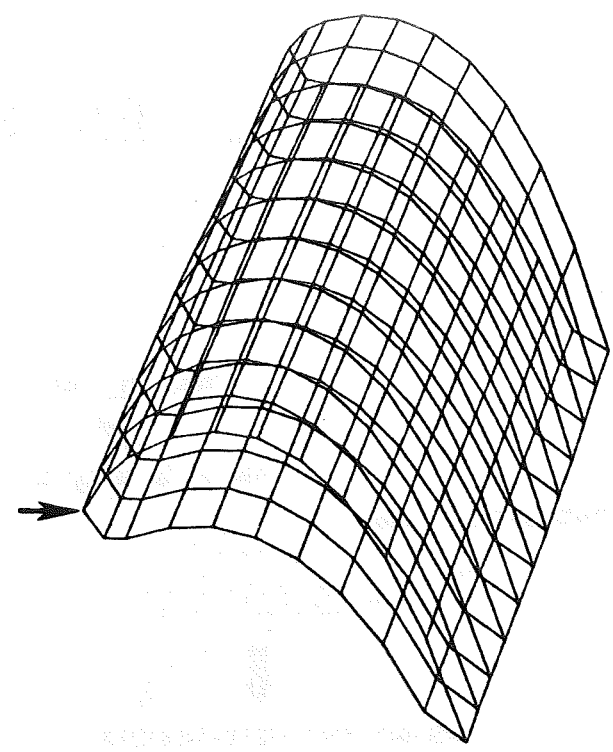
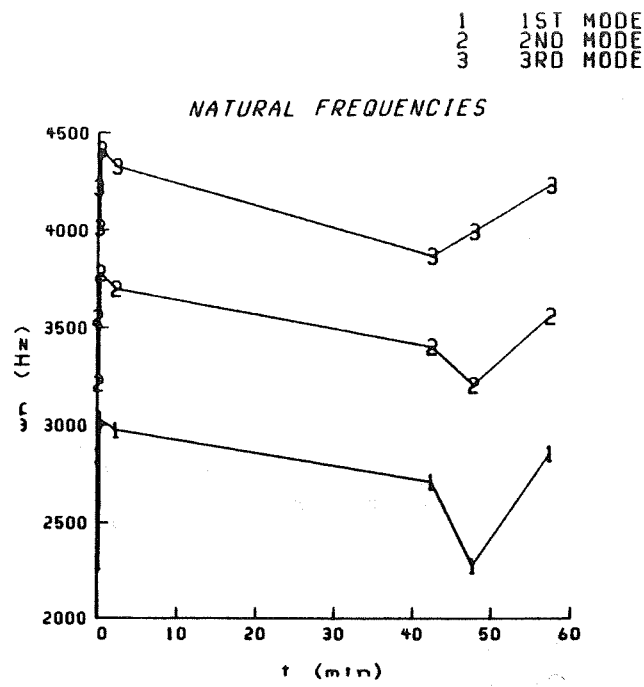


Figure 12 - Variation of Airfoil Natural Frequencies